Segment-interaction in sprint start: Analysis of 3D angular velocity and kinetic energy in elite sprinters

Article *in* Journal of Biomechanics · March 2010

DOI: 10.1016/j.jbiomech.2010.01.044 · Source: PubMed

CITATIONS
47

READS
783

8 authors, including:

Jean Slawinski
Institut National du Sport, de l'Expertise et de la Performance
67 PUBLICATIONS **1,659** CITATIONS

SEE PROFILE

Laurence Cheze
Claude Bernard University Lyon 1
297 PUBLICATIONS **2,700** CITATIONS

SEE PROFILE

Raphael Dumas
University of Lyon - IFSTTAR
206 PUBLICATIONS **2,401** CITATIONS

SEE PROFILE

Journal of Biomechanics 43 (2010) 1494–1502

Contents lists available at ScienceDirect

Journal of Biomechanics

journal homepage: www.elsevier.com/locate/jbiomech
www.JBiomech.com

Segment-interaction in sprint start: Analysis of 3D angular velocity and kinetic energy in elite sprinters

J. Slawinski [a,*], A. Bonnefoy [a], G. Ontanon [a], J.M. Leveque [a], C. Miller [a], A. Riquet [a], L. Chèze [b,c], R. Dumas [b,c]

[a] Scientific expertise centre, TeamLagardere, Jean Bouin Stadium, General Sarrail Avenue 26, 75016 Paris, France
[b] Université Lyon 1, F-69622 Villeurbanne, France
[c] INRETS, UMR_T9406 Laboratoire de Biomécanique et Mécanique des Chocs, F-69675 Bron, France

ARTICLE INFO

Article history:
Accepted 21 January 2010

Keywords:
3D angular velocity
Kinetic energy
Sprint
Motion analysis
Elite athletes

ABSTRACT

The aim of the present study was to measure during a sprint start the joint angular velocity and the kinetic energy of the different segments in elite sprinters. This was performed using a 3D kinematic analysis of the whole body. Eight elite sprinters (10.30 ± 0.14 s 100 m time), equipped with 63 passive reflective markers, realised four maximal 10 m sprints start on an indoor track. An opto-electronic Motion Analysis® system consisting of 12 digital cameras (250 Hz) was used to collect the 3D marker trajectories. During the pushing phase on the blocks, the 3D angular velocity vector and its norm were calculated for each joint. The kinetic energy of 16 segments of the lower and upper limbs and of the total body was calculated. The 3D kinematic analysis of the whole body demonstrated that joints such as shoulders, thoracic or hips did not reach their maximal angular velocity with a movement of flexion–extension, but with a combination of flexion–extension, abduction–adduction and internal–external rotation. The maximal kinetic energy of the total body was reached before clearing block (respectively, 537 ± 59.3 J vs. 514.9 ± 66.0 J; $p \leq 0.01$). These results suggested that a better synchronization between the upper and lower limbs could increase the efficiency of pushing phase on the blocks. Besides, to understand low interindividual variances in the sprint start performance in elite athletes, a 3D complete body kinematic analysis shall be used.

1. Introduction

Humans can engage in many different actions called "explosive" as jumping, kicking and throwing. Common features of explosive movements are the short duration and high angular velocities. In Athletics, the most explosive kind of action is the "starting block phase" (the time when the sprinter is in contact with the blocks) of a 60 or 100 m sprint. The aim of this phase is to create the greatest horizontal velocity of the centre of mass (CM) at the clearing block (VCM_{clear}). Indeed, many studies (Mero et al., 1992; Harland and Steele, 1997; Čoh et al., 2006; Slawinski et al., 2010) have clearly shown that better performances on 100 m are obtained for higher VCM_{clear} and thus depend on the ability of the sprinter to create a great impulse in the shortest time. To understand this ability, some works were interested in the transformation of joint rotations into the desired translation (Bobbert and van Ingen Schenau, 1988; Ingen Schenau, 1989; de Koning et al., 1991). They hypothesised that the centre of mass (CM) translation of multi-joint system is due to the transformation of the joint's rotations into the desired translation.

This transformation during push-off action has been studied during squat jump exercise (Bobbert and van Ingen Schenau, 1988; Bobbert et al., 1996; Ridderikhoff et al., 1999; Mathiyakom et al., 2006), during skating (de Koning et al., 1991), during the first steps of sprinting (Jacobs and van Ingen Schenau, 1992) and during the starting block phase (Mero et al., 2006). Mero et al. (2006) suggested that to reach high velocity of the centre of mass at the clearing block, a greater peak ankle joint moment and power is necessary.

However, all these studies, about joint moment and joint power, used 2D kinematical analysis and restricted their investigations to lower limbs. To understand the contribution of each segment in the transformation of segmental rotation to the translational movement of the CM during the sprint start, the use of a whole body 3D model is essential to have some information about the influence of the movement in the three planes.

The aim of the present study was to measure the joint angular velocity (JAV) and the kinetic energy (KE) of the different segments in elite sprinters using a 3D kinematic analysis of the whole body. This study will respect the joint coordinate system and hypothesised that JAV and KE of the different segments shall explain the contribution of each segment in the transformation of segmental rotations to the translational movement.

* Corresponding author. Tel.: +33 1 40 71 13 86; fax: +33 1 40 71 13 94.
E-mail address: jean.slawinski@teamlagardere.com (J. Slawinski).

0021-9290/$ - see front matter © 2010 Elsevier Ltd. All rights reserved.
doi:10.1016/j.jbiomech.2010.01.044

2. Materials and methods

2.1. Subjects

Eight elite sprinters gave their informed written consent to participate in the study. Their age, body mass, height and personal best times over 100 m are presented in Table 1. Performance times over 100 m ranged between 10.07 and 10.43 s. This study conformed to the recommendations of the Declaration of Helsinki, and had been approved by the local Ethics Committee.

2.2. Experimental procedure

Each subject realised four maximal 10 m sprint starts on an indoor track using starting blocks. Only the pushing phase on the block was analysed. This phase corresponds to the time from the first movement of the set position to the clearing block (Fig. 1). All the data were re-sampled, using a cubic spline interpolation, on 100% of the pushing phase to be further plotted (the clearing block is 100% of the pushing phase). All the trials were used for further analysis.

2.3. Segment coordinate systems

For this study 16 rigid segments were used in order to model the body: head–neck, thorax, abdomen, pelvis, front and rear arms, forearms, hands, thighs, legs and feet. Thus, the trunk was divided into three segments: the thorax, the abdomen and the pelvis. Rear and front joints were, respectively, associated with the side of the rear and the front legs in the starting blocks.

For each segment anatomical landmarks were used (Fig. 2). The choice of the anatomical landmarks (see Appendix A) was based on the study of Dumas et al. (2007) and according to ISB proposal (Wu et al., 2002, 2005).

The 3D trajectories of the anatomical landmarks have been recorded using an optoelectronic system during the pushing block phase and obtained in the Inertial Coordinate System (ICS) (Wu and Cavanagh, 1995). Then, the joint coordinate centres (JCC) and the segment coordinate systems (SCS) were built on each body segment at each point time. From these SCS, the rotations sequences proposed by the ISB (Wu et al., 2002, 2005) were used to describe kinematics during the pushing block phase of eleven joints (see Appendix B).

2.4. Kinetic energy and norm of the 3D joint angular velocity

The 3D angular velocity of the proximal and distal segments was obtained using the homogenous matrix algebra (Legnani et al., 1996; Doriot and Cheze, 2004). From

Table 1
Characteristics of the sprinters.

	Height (cm)	Weight (kg)	Age (years)	100-m time (s)
Elite sprinters ($\pm$SD)	182.1 ± 7.7	79.5 ± 8.9	24.1 ± 3.0	10.30 ± 0.14

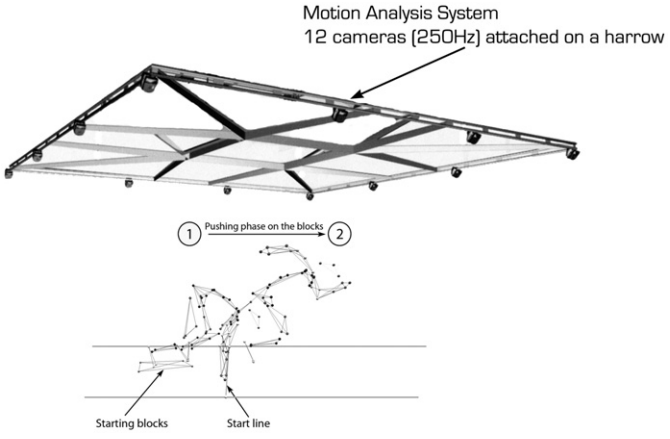

Fig. 1. Experimental design: 1—corresponds to the "set" position, 2—corresponds to the clearing block.

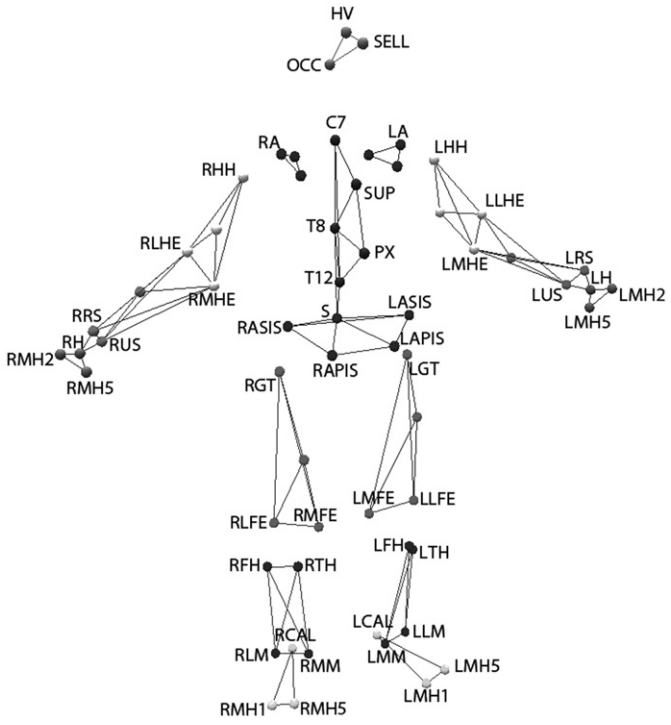

Fig. 2. Position of anatomical landmarks in initial static position. The names of the anatomical landmarks are detailed in Appendix A. The landmarks without name are used to improve the tracking procedure.

matrix $T_{i/0}$ defining both the orientation and the position of the ith SCS with respect to an Inertial Coordinate System (ICS), the velocity matrix was calculated:

$$W_{i/0} = \begin{bmatrix} & \tilde{\Omega}_{i/0} & & \vec{V}_{i/0}(O_i) \\ 0 & 0 & 0 & 0 \end{bmatrix} = \left(\dot{T}_{i/0}\right)(T_{i/0})^{-1}$$

with $(T_{i/0})^{-1}$ the inverse matrix and $\left(\dot{T}_{i/0}\right)$ the first order derivative of the matrix $T_{i/0}$ (computed using a centred fourth-order finite difference followed by a low-pass filtering).

In this velocity matrix, the last column, $\vec{V}_{i/0}(O_i)$ is the linear velocity of the point O_i, embedded in the ith segment and coinciding with the origin of ICS at the considered instant of time. Besides, $\tilde{\Omega}_{i/0}$ is a skew-symmetric matrix of the segment angular velocity $\vec{\Omega}_{i/0}$. The linear velocity of the segment centre of mass can be deduced:

$$\vec{V}_{i/0}(G_i) = \vec{V}_{i/0}(O_i) + \tilde{\Omega}_{i/0} \times \overrightarrow{O_iG_i}$$

with $\overrightarrow{O_iG_i}$ the position of the segment centre of mass in the ICS (estimated by regressions in the SCS (Dumas et al., 2007) and then transformed using $T_{i/0}$).

The kinetic energy (KE) was therefore computed for each body segment, for the total body, for the upper limb (front and rear arm, fore arm and hand), lower limb (front and rear thigh, leg and foot) and head–trunk segment (head–neck, thorax, abdomen and pelvis) by

$$\mathrm{KE} = \sum_{i=1}^{16} \left((1/2) m_i (\overrightarrow{V_{i/0}}(G_i))^2 + \frac{1}{2} \vec{\Omega}_{i/0} \cdot I_i \vec{\Omega}_{i/0} \right)$$

where m_i is the segment mass, $\mathbf{I}_i$ the segment inertia tensor in the ICS (estimated by regressions in the SCS (Dumas et al., 2007) and then transformed using $T_{i/0}$). The maximal values of the KE, $\mathrm{KE_{max}}$, and the time corresponding ($\%\mathrm{TKE_{max}}$) were calculated for each body segment and for the total body. The sum between each $\mathrm{KE_{max}}$ of each body segment was calculated.

The joint angular velocity and its norm $\|\vec{\Omega}_{i/i-1}\|$ (NJAV) were computed from proximal and distal segment angular velocities:

$$\vec{\Omega}_{i/i-1} = \vec{\Omega}_{i/0} - \vec{\Omega}_{i-1/0}$$

The contribution of each degree of freedom was also computed. For this, the joint angular velocity was projected on each axis of the joint coordinate system

(JCS) in order to retrieve the Euler angles derivatives $\left(\dot{\alpha},\dot{\beta},\dot{\gamma}\right)$:

$$\vec{\Omega}_{i/i-1}=\underbrace{\frac{\left(\vec{e_2}\times\vec{e_3}\right)\bullet\vec{\Omega}_{i/i-1}}{\left(\vec{e}_1\times\vec{e_2}\right)\bullet\vec{e_3}}}_{\dot{\alpha}}\vec{e_1}+\underbrace{\frac{\left(\vec{e_3}\times\vec{e_1}\right)\bullet\vec{\Omega}_{i/i-1}}{\left(\vec{e}_1\times\vec{e_2}\right)\bullet\vec{e_3}}}_{\dot{\beta}}\vec{e_2}+\underbrace{\frac{\left(\vec{e_1}\times\vec{e_2}\right)\bullet\vec{\Omega}_{i/i-1}}{\left(\vec{e}_1\times\vec{e_2}\right)\bullet\vec{e_3}}}_{\dot{\gamma}}\vec{e_3}$$

where $\vec{e_1}$ is a selected axis from the matrix $T_{i-1/0}$, and $\vec{e_3}$ is a selected axis from the matrix $T_{i/0}$ and $\vec{e_2}=\vec{e_{''}}\times\vec{e_1}$.

This procedure was preferred to the classical computation of the Euler angles than can be prone to singularity and discontinuity. Moreover, doing so, all the results are uniformly obtained from the same angular velocity computations. These values, called Euler angular velocity (EAV), could be used, in addition to the numerical value of NJAV, to know which degree of freedom (flexion/extension, adduction/abduction and internal/external rotation) is more important during the pushing phase of the sprint start. From the NJAV, the maximal values, $NJAV_{max}$ were calculated to analyse the data.

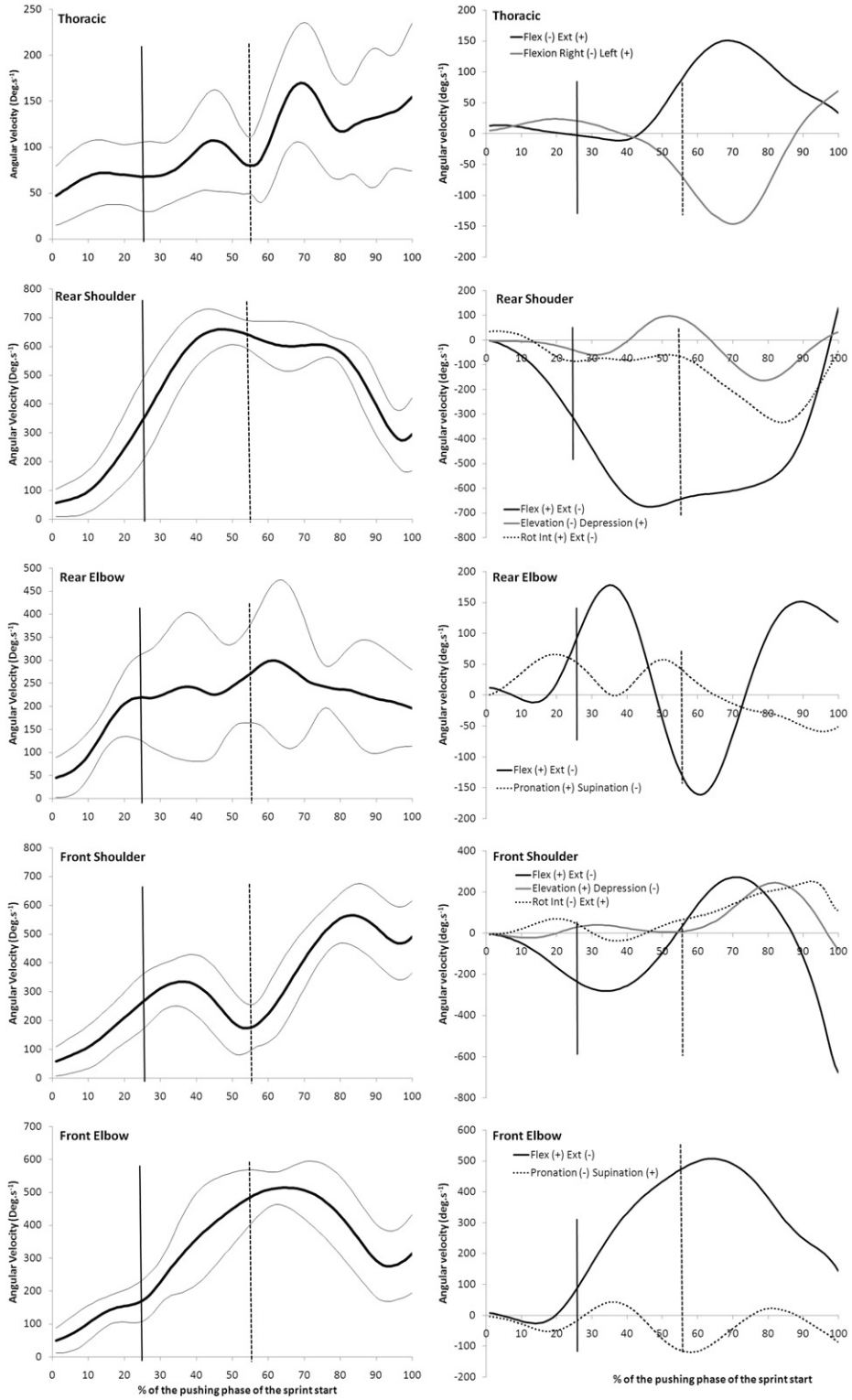

Fig. 3. Joint angular velocity of the upper joints. The left-hand panel represents the norm of the joint angular velocity (NJAV) and the right-hand panel represents the 3D Euler angular velocity (EAV). The vertical bold line indicates the take-off of the hands (around 25% of the pushing phase) and the vertical dotted line indicates the clearing of the block of the rear foot (around 55% of the pushing phase).

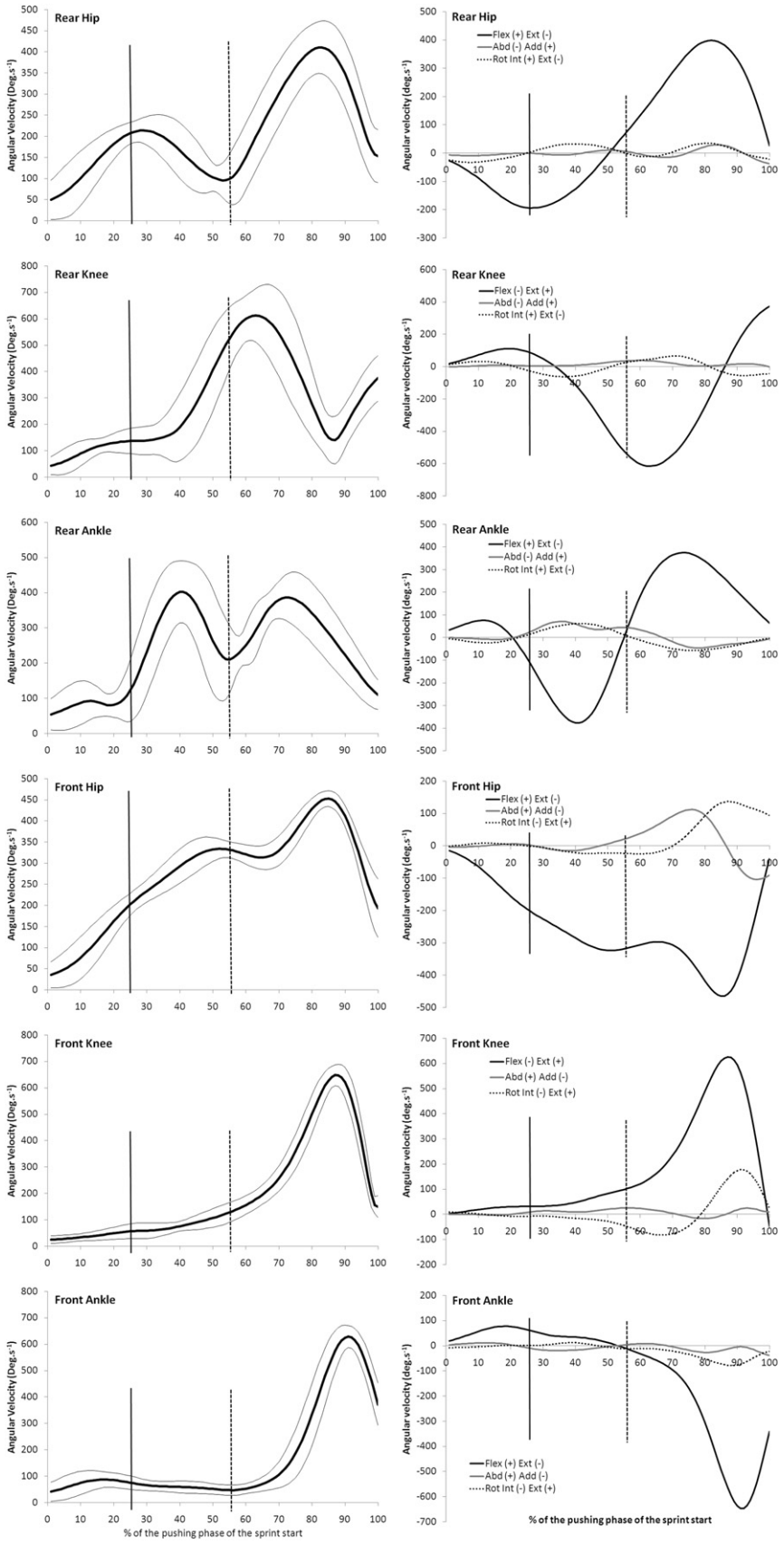

Fig. 4. Joint angular velocity of the lower joints. The left-hand panel represents the norm of the joint angular velocity (NJAV) and the right-hand panel represents the 3D Euler angular velocity (EAV). The vertical bold line indicates the take-off of the hands (around 25% of the pushing phase) and the vertical dotted line indicates the clearing of the block of the rear foot (around 55% of the pushing phase).

2.5. Statistical analysis

All data are presented as means plus or minus standard deviations. After a normality test, comparison of $NJAV_{max}$ between the different joints was performed with a repeated ANOVA. Paired and unpaired Student tests were used to compare kinetic energy. All significant differences reported are at $p \leq 0.01$.

Table 2
Mean maximal norm of joint angular velocity ($NJAV_{max}$).

	$NJAV_{max}$ ($^\circ s^{-1}$) ($\pm$SD)
Thoracic	220.2 ± 57.5
Rear shoulder	703.1 ± 49.6
Rear elbow	376.9 ± 141.8
Front shoulder	641.7 ± 79.5
Front elbow	562.4 ± 78.8
Rear hip	425.7 ± 61.0
Rear knee	651.4 ± 112.3
Rear ankle	462.9 ± 74.7
Front hip	456.3 ± 17.7
Front knee	660.2 ± 40.5
Front ankle	641.5 ± 44.9

3. Results

3.1. Maximal norm of the joint angular velocity ($NJAV_{max}$)

Figs. 3 and 4 show the evolution of the norm of joint angular velocity and the 3D Euler angular velocity of the different joints during the pushing phase on the blocks. During the start phase, the thoracic joint (the joint between the thorax and the abdomen) has a significantly lower maximal angular velocity than the other joints ($220.2 \pm 57.5^\circ s^{-1}$). Inversely, the rear shoulder maximal angular velocity is significantly higher than the other joints ($703.1 \pm 49.6^\circ s^{-1}$). The values of $NJAV_{max}$ are presented in Table 2.

3.2. Maximal kinetic energy (KE_{max})

The evolution of the kinetic energy of the different segments, of the lower limbs, the upper limbs, the head–trunk segments and of the total body is presented in Figs. 5–8. Values of KE_{max} of the different segments are presented in Table 3. The KE_{max} of the total body was significantly greater than the KE of the total body at the

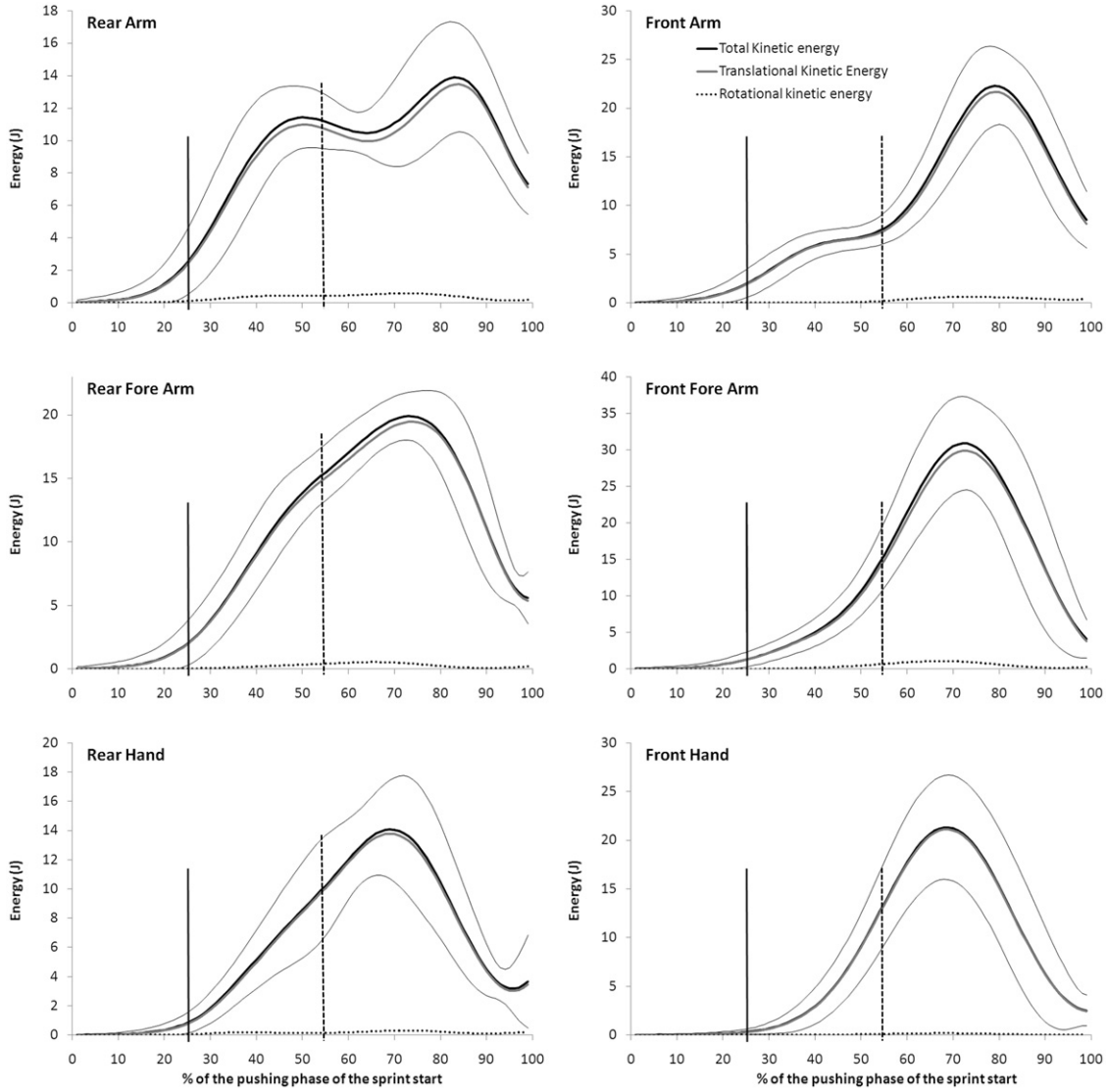

Fig. 5. Rotational, translational and total kinetic energy of the upper limb segments (rear and front arm, fore arm and hand). The vertical bold line indicates the take-off of the hands (around 25% of the pushing phase) and the vertical dotted line indicates the clearing of the block of the rear foot (around 55% of the pushing phase).

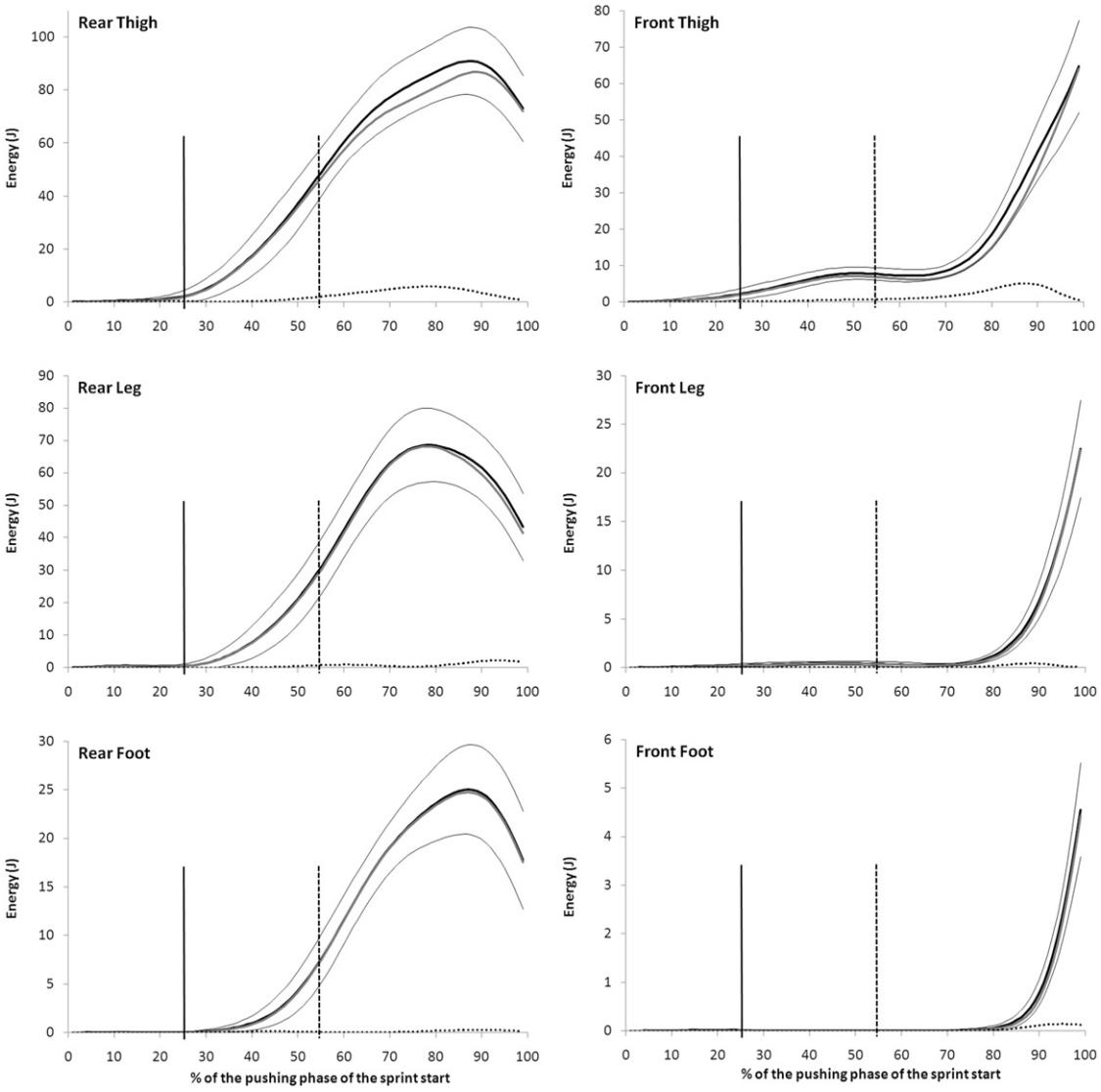

Fig. 6. Rotational, translational and total kinetic energy of the lower limb segments (rear and front thigh, leg and foot). The vertical bold line indicates the take-off of the hands (around 25% of the pushing phase) and the vertical dotted line indicates the clearing of the block of the rear foot (around 55% of the pushing phase).

clearing block (537 ± 59.3 J vs. 514.9 ± 66.0 J; $p \leq 0.01$). Moreover, KE_{max} of the total body was significantly lower than the sum of KE_{max} of each segment (Table 3; $p \leq 0.01$), as the maximum values of KE are not reached at the same time for all the body segments (see Appendix C). The upper limbs develop a lower KE_{max} than the lower limbs or the head–trunk segments (Table 3; $p \leq 0.01$). However, KE_{max} of the head–trunk segments was not significantly different of the KE_{max} of the lower limbs Fig. 8.

3.3. Time of maximal kinetic energy (%TKE_{max})

The time of maximal kinetic energy of the total body was reached at 91.9 ± 3.5% of the pushing phase of the sprint start. The $\%TKE_{max}$ of the different segments were not reached at the same time. The head–neck, the thorax, the abdomen and the pelvis reached $\%TKE_{max}$ around 96–99% of the pushing phase of the sprint start. Front and rear arms reached $\%TKE_{max}$ around 67–80% of the pushing phase of the sprint start. Rear leg reached $\%TKE_{max}$ around 79–88% and front leg at the clearing block. Upper limbs reach KE_{max} sooner than the lower limbs or the head–trunk segments (Table 3; $p \leq 0.01$).

4. Discussion

Several publications dealt with the technique and biomechanics of the sprint start. Indeed, in general, high performance levels over 100 m correlate with correspondingly high performance levels in the block start and acceleration phase of the race. However, it appears that the majority of these publications were based on 2D analysis. That is why the aim of the present study was to analyse the pushing block phase in high-level athletes with a 3D biomechanical model calculating the joint angular velocity and the kinetic energy, respecting the ISB recommendations. The idea was to use the relevance of the 3D model in order to analyse the body organization of the high-level athletes and to have some information about the influence of the movements in the three planes during a specific explosive and horizontal action as the pushing block phase.

4.1. The norm of the joint angular velocity

Actually, it appears that the norm of the joint angular velocity was never studied during the pushing block phase for the lower

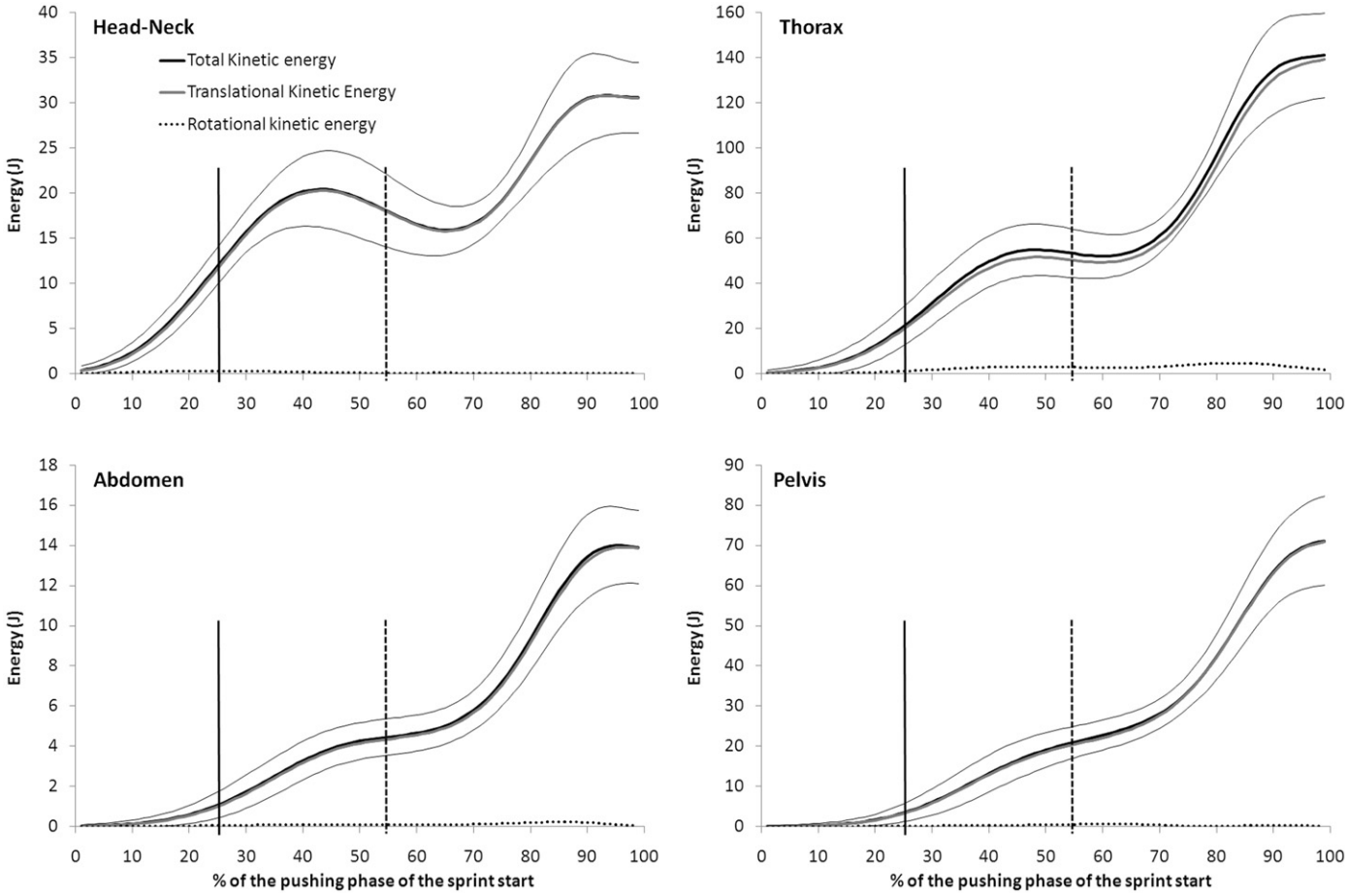

Fig. 7. Rotational, translational and total kinetic energy of the segments of the head–trunck (head–neck, thorax, abdomen and pelvis). The vertical bold line indicates the take-off of the hands (around 25% of the pushing phase) and the vertical dotted line indicates the clearing of the block of the rear foot (around 55% of the pushing phase).

and upper limbs. From the previously published literature, only the 2D joint angular velocities were described during the first step after the pushing block phase (Jacobs and van Ingen Schenau, 1992; Johnson and Buckley, 2001; Hunter et al., 2004; Bezodis et al., 2008). These studies found hip angular velocities from 700 to 900° s^{-1}, knee angular velocities from 550 to 900° s^{-1} and ankle angular velocities from 1000 to 1400° s^{-1}. The present study demonstrated that the maximal norm of the joint angular velocities ($NJAV_{max}$) of the hip, knee and ankle are lower (comprised between 350 and 600° s^{-1}; Table 2) during the pushing block phase than during the first step of the run.

In order to better analyse the $NJAV_{max}$ of the different joints, the 3D Euler angular velocities (EAV) were calculated. Indeed, the idea was to know which movement produces the NJAV during the pushing block phase independently of the numerical values. Thus, it appears that the $NJAV_{max}$ of the front hip and knee is mainly associated to a movement of extension (Fig. 3). The movement of the ankle is more complex, because the first half of the pushing block phase is a flexion and the second one is an extension. The analysis of the EAV shows also, for the hip and the knee, that the extension is not the unique movement which participates to the creation of $NJAV_{max}$. Indeed, the hip combines an external rotation and a sequence of abduction, adduction. The knee associates to the extension a movement of external rotation.

Concerning the rear lower limb, the 3D analysis of the EAV (Fig. 3), shows that between 0% and 20% of the pushing block phase, rear hip and knee have velocities are due to an extension movement, while ankle velocity is linked to a flexion movement. From 20% to 35% of the pushing block phase, the hip, knee and ankle velocities are linked to an extension movement. Finally, from 35% to the clearing of the rear foot (around 50%) hip and ankle velocities are linked to an extension movement contrary to the knee.

The fact that the front and rear ankle joints have the same action during this movement can be remarkable. Indeed, the front and rear ankles combine a flexion–extension movement which reveals a strength-shortening cycle. However, the duration of the ankle's flexion is greater for the rear ankle (50% of pushing block phase) than for the front ankle (20% of the pushing block phase). From a muscular point of view, the triceps surae and the gastrocnemius of the both legs acted eccentrically before their concentric phase which indicates a pliometric action of both ankles. This result was already highlighted by Mero and Komi (1990) for well trained sprinters. However, the flexion of the ankle before extension, rather than an only extension, leads up to a waste of time that could be unfavourable to a good performance on 100 m.

Concerning the rear upper limb (Fig. 3), the $NJAV_{max}$ of the rear shoulder is greater than that of the other joints. Contrary to the lower limbs, it is important to note that standard deviations for the upper limbs are great. Thus the organization of the upper limbs is more variable between runners than that of the lower limbs. However, it could be possible to recognize three patterns of motion for the NJAV of the upper limbs in relation with the morphological properties of the athletes (height) and their techniques during the start.

The 3D analysis of the EAV (Fig. 3) shows that the velocity of the rear shoulder is linked to an extension movement that starts

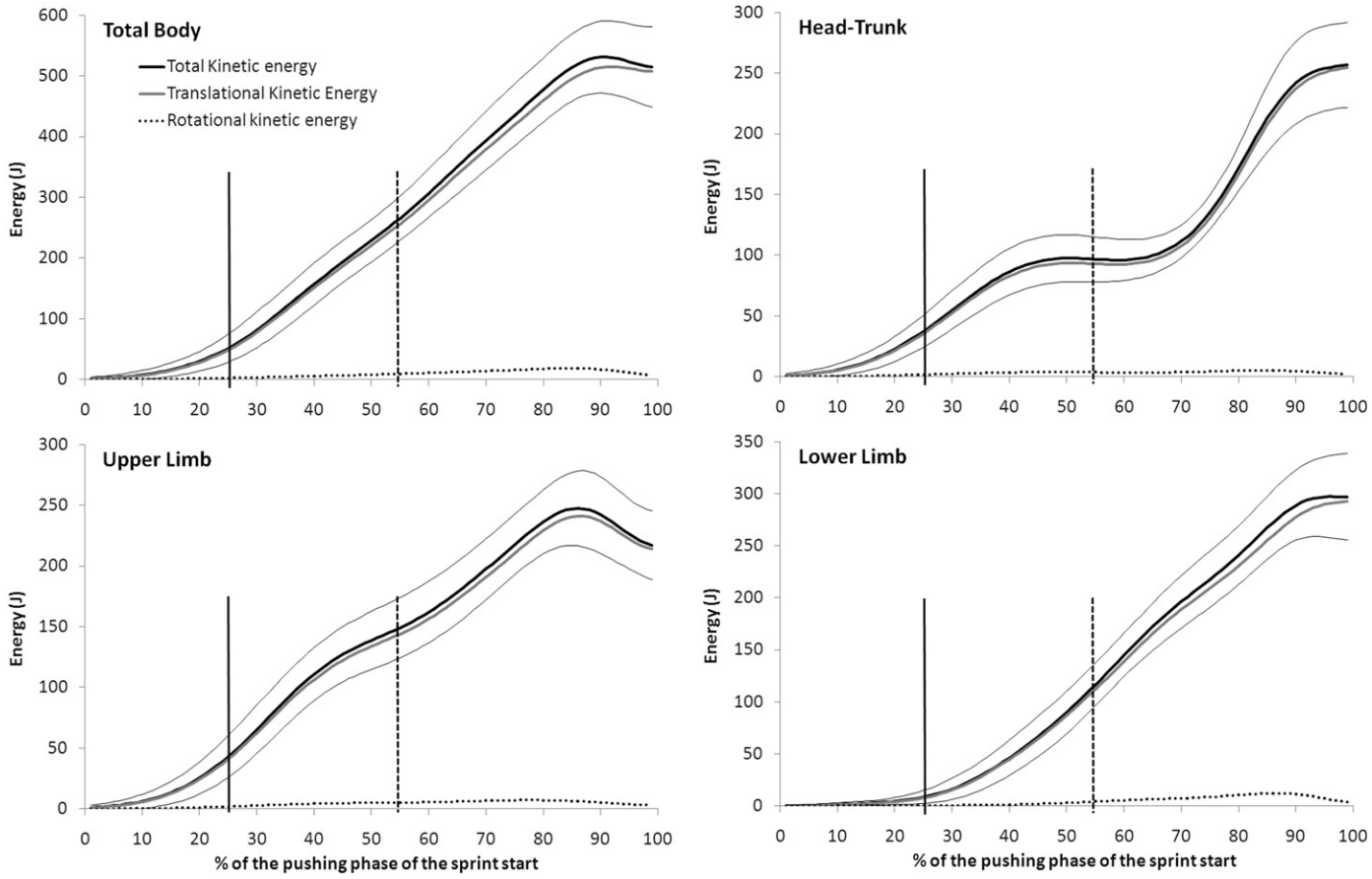

Fig. 8. Rotational, translational and total kinetic energy of the total body, upper and lower limbs. The vertical bold line indicates the take-off of the hands (around 25% of the pushing phase) and the vertical dotted line indicates the clearing of the block of the rear foot (around 55% of the pushing phase).

Table 3
Maximal kinetic energy (KE_{max}) of each segment and time of maximal kinetic energy ($\%TKE_{max}$). The sum of KE_{max} of each segment is not equal to the KE_{max} value of the lower and upper limbs, the head–trunk segment and the total body, because the KE_{max} of each segment are not reached at the same time during the movement (see Appendix C).

	KE_{max} (J) ($\pm$SD)	**$\%TKE_{max}$ (%)** ($\pm SD$)
Head–neck	31.6 ± 5.0	96.4 ± 4.0
Thorax	142.5 ± 20.8	98.4 ± 2.8
Abdomen	14.3 ± 2.0	97.1 ± 3.5
Rear arm	14.7 ± 3.2	80.0 ± 11.6
Rear fore arm	20.5 ± 2.7	74.3 ± 4.8
Rear hand	15.0 ± 3.5	67.8 ± 5.4
Front arm	23.3 ± 4.1	81.0 ± 4.0
Front fore arm	32.3 ± 6.9	74.1 ± 4.3
Front hand	22.2 ± 5.8	70.1 ± 4.5
Pelvis	71.3 ± 10.9	98.9 ± 1.9
Rear thigh	91.4 ± 12.4	86.4 ± 4.7
Rear leg	69.1 ± 11.1	79.4 ± 4.2
Rear foot	25.3 ± 4.5	88.3 ± 3.1
Front thigh	64.7 ± 12.6	100.0 ± 0.0
Front leg	22.5 ± 5.0	100.0 ± 0.0
Front foot	4.6 ± 1.0	100.0 ± 0.0
Upper limbs	119.5 ± 19.1[a]	74.9 ± 3.8[a]
Lower limbs	230.8 ± 30.0	95.8 ± 4.4
Trunk	258.3 ± 36.8	98.3 ± 2.4
Total body	537.0 ± 59.3	91.9 ± 3.5
$\sum$segments	665.3 ± 87.0[b]	

[a] Significantly different from the lower limb and the trunk.
[b] Significantly different from the lower limb and the total body.

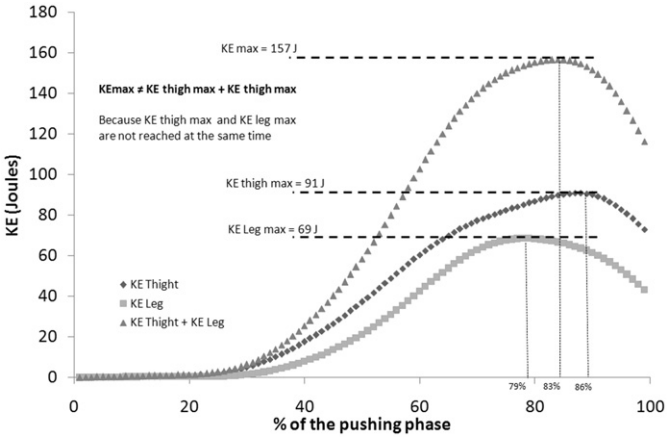

Fig. 9. Example of calculation of the kinetic energy (KE) of two limbs.

at the beginning of the pushing phase. When the hands are on the ground, the extension is mainly associated with the raising of the thorax. Then, the rear shoulder moves on the back and $NJAV_{max}$ is associated to a movement of extension. The rear elbow begins the movement by a combination extension and pronation (Fig. 3). This movement of extension suggested that hands have an action on the ground.

4.2. Kinetic energy

Total kinetic energy is a useful tool to describe the efficiency of a movement because KE must be maximized to increase the efficiency of the movement (Hubley and Wells, 1983). The result shows that the lower limbs and the head–trunk segments are the two main segments which contribute to the KE of the total body. Upper limbs contribute for 22% to the KE of the total body. This demonstrates that their actions in the pushing phase on the blocks are not negligible. Moreover, the KE of upper limbs reaches its maximum around 75% of the pushing phase on the blocks and then decreases. The increase of the KE of the lower limbs begins later (around the take-off of the hands) and rises until the clearing block. The KE of the head–trunk segments increases from the beginning until the clearing block. This suggests that the upper limbs and the head–trunk segments contribute to increase the KE of the total body at the beginning of the movement and that the lower limbs and the head–trunk segments contribute to limit the decrease of KE of the total body at the clearing block. These results highlight the importance of the synchronization between the upper and lower limbs to increase the efficiency of the pushing block phase (Fig. 9). Indeed, three main conditions must be respected to increase the KE during the pushing phase on the blocks.

The first one is that the rotational kinetic energy represents a negligible part of the total kinetic energy and those for all the segments. This means that all segments contribute to create translational energy at the clearing block.

The second one is that KE_{max} of the total body must be the greatest possible. The present data suggest that KE_{max} of the total body could be greater. Indeed, if each segment reaches its KE_{max} at the same time, KE_{max} of the total body would be 24% greater.

The third condition to maximize the production of KE is that KE_{max} of the total body is reached at the clearing block because during the subsequent flying phase an increase of KE is generally low or nonexistent in running. The present data show that the maximal kinetic energy is not reached at the clearing block. Indeed, the reduction of KE before the clearing block is mainly associated with the decrease of the KE of the upper limb energy of both arms and the energy of the rear leg.

5. Conclusion

The norm of the angular velocity demonstrated that joints such as shoulders, thoracic or hips did not reach their maximal angular velocity with a movement of flexion–extension, but with a combination of flexion–extension, abduction–adduction and internal–external rotation. The kinetic energy approach of the pushing phase on the blocks supplies useful information concerning upper and lower limbs contributions to the translation of the body in the forward direction. Then, the results demonstrated that complex movement such as sprint start must be studied using a 3D kinematical analysis.

Conflict of interest statement

None.

Appendix A. Supplementary material

Supplementary data associated with this article can be found in the online version at doi:10.1016/j.jbiomech.2010.01.044.

References

Bezodis, I.N., Kerwin, D.G., Salo, A.I., 2008. Lower-limb mechanics during the support phase of maximum-velocity sprint running. Medicine Science in Sports Exercise 40, 707–715.

Bobbert, M.F., Gerritsen, K.G., Litjens, M.C., Van Soest, A.J., 1996. Why is countermovement jump height greater than squat jump height? Medicine Science in Sports Exercise 28, 1402–1412.

Bobbert, M.F., van Ingen Schenau, G.J., 1988. Coordination in vertical jumping. Journal of Biomechanics 21, 249–262.

Čoh, M., Tomažin, K., Štuhec, S., 2006. The biomechanical model of the sprint start and block acceleration. Physical Education and Sport 4, 103–114.

de Koning, J.J., de Groot, G., van Ingen Schenau, G.J., 1991. Coordination of leg muscles during speed skating. Journal of Biomechanics 24, 137–146.

Doriot, N., Cheze, L., 2004. A three-dimensional kinematic and dynamic study of the lower limb during the stance phase of gait using an homogeneous matrix approach. IEEE Transactions on Biomedical Engineering 51, 21–27.

Dumas, R., Cheze, L., Verriest, J.P., 2007. Adjustments to McConville et al. and Young et al. body segment inertial parameters. Journal of Biomechanics 40, 543–553.

Harland, M.J., Steele, J.R., 1997. Biomechanics of the sprint start. Sports Medicine 23, 11–20.

Hubley, C.L., Wells, R.P., 1983. A work-energy approach to determine individual joint contributions to vertical jump performance. European Journal of Applied Physiology 50, 247–254.

Hunter, J.P., Marshall, R.N., McNair, P.J., 2004. Segment-interaction analysis of the stance limb in sprint running. Journal of Biomechanics 37, 1439–1446.

Ingen Schenau, G.J., 1989. From rotation to translation: constraints on multi-joint movements and the unique action of biarticular muscles. Human Movement Science, 301–337.

Jacobs, R., van Ingen Schenau, G.J., 1992. Intermuscular coordination in a sprint push-off. Journal of Biomechanics 25, 953–965.

Johnson, M.D., Buckley, J.G., 2001. Muscle power patterns in the mid-acceleration phase of sprinting. Journal of Sports Science 19, 263–272.

Legnani, G., Casolo, F., Righettini, P., Zappa, B., 1996. A homogeneous matrix approach to 3D kinematics and dynamics. Mechanisms and Machine Theory 31, 573–587.

Mathiyakom, W., McNitt-Gray, J.L., Wilcox, R., 2006. Lower extremity control and dynamics during backward angular impulse generation in backward translating tasks. Experimental Brain Research 169, 377–388.

Mero, A., Komi, P.V., 1990. Reaction time and electromyographic activity during a sprint start. European Journal of Applied Physiology 61, 73–80.

Mero, A., Komi, P.V., Gregor, R.J., 1992. Biomechanics of sprint running. A review. Sports Medicine 13, 376–392.

Mero, A., Kuitunen, S., Harland, M., Kyrolainen, H., Komi, P.V., 2006. Effects of muscle–tendon length on joint moment and power during sprint starts. Journal of Sports Science 24, 165–173.

Ridderikhoff, A., Batelaan, J.H., Bobbert, M.F., 1999. Jumping for distance: control of the external force in squat jumps. Medicine Science in Sports Exercise 31, 1196–1204.

Slawinski, J., Bonnefoy, A., Leveque, J., Ontanon, G., Riquet, A., Dumas, R.,Chèze, L., 2010. Kinematic and kinetic comparison of elite and well-trained sprinter during sprint start. Journal of Strength and Conditioning Research, in press, doi:10.1519/JSC.0b013e3181ad3448.

Wu, G., Cavanagh, P.R., 1995. ISB recommendations for standardization in the reporting of kinematic data. Journal of Biomechanics 28, 1257–1261.

Wu, G., Siegler, S., Allard, P., Kirtley, C., Leardini, A., Rosenbaum, D., Whittle, M., D'Lima, D.D., Cristofolini, L., Witte, H., Schmid, O., Stokes, I., 2002. ISB recommendation on definitions of joint coordinate system of various joints for the reporting of human joint motion—Part I: ankle, hip, and spine. International Society of Biomechanics. Journal of Biomechanics 35, 543–548.

Wu, G., van der Helm, F.C., Veeger, H.E., Makhsous, M., Van Roy, P., Anglin, C., Nagels, J., Karduna, A.R., McQuade, K., Wang, X., Werner, F.W., Buchholz, B., 2005. ISB recommendation on definitions of joint coordinate systems of various joints for the reporting of human joint motion—Part II: shoulder, elbow, wrist and hand. Journal of Biomechanics 38, 981–992.

Appendix A

Kinematic data of the 16 rigid body segments were collected using an optoelectronic Motion Analysis® system (Santa Rosa, California) consisting of 12 digital cameras. The scanning frequency was set to 250 HZ. The Inertial Coordinate System (ICS) origin was placed on the middle of the start lane. Before starting the data collect, the optoelectronic device was calibrated. Each subject was equipped with 62 passive reflective markers (16 mm diameter) glued directly to the skin on anatomical landmarks with a double-sided tape. In order to have a better fixation of the markers, a special spray (recommended by the physiotherapist) was used to improve the gluing and to limit the problem of the sweat of the athletes. After the preparation of the athlete, the first record corresponded to the reference position i.e. the athlete was standing up with the arms outspread (see figure 2). After this record, the athlete realized four maximal sprint starts. The 3D trajectories of the passive reflective markers were computed and then filtered using a bidirectional low-pass filter (Butterworth, fourth-order, with a cut-off frequency of 12 Hz).

Definition of anatomical landmarks from Dumas et al. (2007):

Rigid Body Segments	Anatomical Landmarks used
Head - Neck	HeadVertex (HV) Sellion (SELL) Occiput (OCC)
Thorax and Abdomen	7th Cervicale (C7) 8th Thoracic (T8) 12th Thoracic (T12) Suprasternale (SUP) Processus Xiphoideu (PX) Right and left Acromion (RA and LA)
Pelvis	Sacral (S) Right and Left Antero Superior Iliac Spines (RASIS and LASIS) Right and Left Antero Posterior Iliac Spines (RAPIS and LAPIS)
Right and Left Arm	Right and Left Humerus Head (RHH and LHH) Right and Left Lateral Humeral Epicondyle (RLHE and LLHE) Right and Left Medial Humeral Epicondyle (RMHE and LMHE)
Right and Left Forearm	Right and Left Ulnar Styloids (RUS and LUS) Right and Left Radial Styloids (RRS and LRS)
Right and Left Hand	Right and Left Hand (RH and LH) Right and Left 2nd Metacarpal Head (RMH2 and LMH2) Right and Left 5th Metacarpal Head (RMH5 and LMH5)
Right and Left Thigh	Right and Left Greater Trochanter (RGT and LGT) Right and Left Lateral Femoral Epicondyles (RLFE and LLFE) Right and Left Medial Femoral Epicondyles (RMFE and LMFE)
Right and Left Leg	Right and Left Tibiale Head (RTH and LTH) Right and Left Fibula Head (RFH and LFH) Right and Left Lateral Malleolus (RLM and LLM) Right and Left Medialis Malleolus (RMM and LMM)
Right and Left Foot	Right and Left Calcaneous (RCAL and LCAL) Right and Left 1st Metatarsal Head (RMH1 and LMH1) Right and Left 5^{th} Metatarsal Head (RMH5 and LMH5)

Appendix B

Definition of the Joint Coordinate Centres (JCC) in Anatomical Coordinate Systems (ACS):

Thorax Joint Centre (ToJC): The joint coordinate centre is the *Cervical Joint Centre (CJC)* estimated from C7, SUP, RA and LA, available in the Thorax ACS, using regression equations (Reynolds et al., 1982; Schneider et al., 1983; Reed et al, 1999; Dumas et al, 2007).

Pelvis Joint Centre (PJC): The joint coordinate centre is the *Lumbar Joint Centre (LuJC)* estimated from RASIS, LASIS, and Sacral available in the Pelvis ACS using regression equations (Reynolds et al., 1982; Schneider et al., 1983; Reed et al, 1999; Dumas et al, 2007).

Abdomen Joint Centre (AbJC): The joint coordinate centre is the *Thoracic Joint Centre (ThJC)* estimated from CJC, LuJC in the Abdomen ACS using regression equations (Dumas et al, 2007).

Head and Neck Joint Centre (HNJC): The joint coordinate centre is the *CJC* transformed from the Thorax ACS into the Head ACS.

Arm Joint Centre (ArJC): The joint coordinate centre is the *Shoulder Joint Centre (SJC)* transformed from the thorax ACS to the Arm ACS. The SJC is estimated from C7, SUP, RA and LA available in the Thorax ACS using regression equations (Reynolds et al., 1982; Schneider et al., 1983; Reed et al, 1999; Dumas et al, 2007).

Forearm Joint Centre (FAJC): The joint coordinate centre is the *Elbow Joint Centre (EJC)* estimated as the midpoint between the LHE and MHE. EJC is transformed from the Arm ACS into the Forearm ACS.

Hand Joint Centre (HaJC): The joint coordinate centre is the *Wrist Joint Centre (WJC)* estimated as the midpoint between the US and RS available in the Hand ACS.

Thigh Joint Centre (ThiJC): The joint coordinate centre is the *Hip Joint Centre (HiJC)* estimated from the RASIS, LASIS, and Sacral available in the Pelvis ACS using regression equations (Reynolds et al., 1982; Schneider et al., 1983; Reed et al, 1999; Dumas et al, 2007). The HiJC is transformed from the Pelvis ACS into the Thigh ACS.

Leg Joint Centre (LeJC): The joint coordinate centre is the *Knee Joint Centre (KJC)* estimated as the midpoint between the LFE and MFE. The KJC is transformed from the Thigh ACS to the Leg ACS.

Foot Joint Centre (FoJC): The joint coordinate centre is the *Ankle Joint Centre (AnJC)* estimated as the midpoint between the LM and LL. The AnJC is transformed from the leg ACS to the Foot ACS.

Definition of the Segment Coordinate Systems (SCS)

Pelvis: The origin is the PJC. The Z-axis of the *Pelvis SCS* runs from LASIS to RASIS. The Y- axis is normal to the plane containing the RASIS, the LASIS and the sacral, pointing cranially. The X-axis is the cross product of the Y and Z axes.

Thorax: The origin is the ToJC. The Y-axis of the *Thorax SCS* runs from LuJC (transformed from the Pelvis ACS into the Thorax ACS) to CJC. The Z- axis is normal to the plane

containing the LuJC, CJC and SUP, pointing laterally. The X-axis is the cross product of the Y and Z axes.

Abdomen: The origin is the AbJC. The Y-axis of the *Abdomen SCS* runs from TJC to LJC. The Z- axis is normal to the plane containing the LuJC, CJC and SUP, pointing laterally. The X-axis is the cross product of the Y and Z axes.

Head and Neck: The origin is the HNJC. The Y-axis of the *Head – Neck SCS* runs from the CJC to the HV. The Z-axis is normal to the plane containing HV, the CJC and SEL, pointing laterally. The X-axis is the cross product between the Y and Z axes.

Arm: The origin is the ArJC. The Y-axis of the *Arm SCS* runs from the EJC to the SJC. The X-axis is normal to the plane containing SJC, LHE and MHE, pointing anteriorly. Z –axis is the cross product between the X and Y axes.

Forearm: The origin is the FAJC. The Y-axis of the *Forearm SCS* runs from the WJC to the EJC. The X-axis is normal to the plane containing EJC, US and RS, pointing anteriorly. Z – axis is the cross product between the X and Y axes.

Hand: The origin is the HaJC. The Y-axis of the *Hands SCS* runs from the midpoint between the MH2 and the MH5. The X-axis is normal to the plane containing WJC, MH2 and MH5, pointing anteriorly. Z –axis is the cross product between the X and Y axes.

Thigh: The origin is the ThiJC. The Y-axis of the *Thigh SCS* runs from the KJC to the HiJC. The X-axis is normal to a plane containing the HiJC, LFE and MFE pointing anteriorly. The Z-axis is the cross product of the X and Y axes.

Leg: The origin is the LeJC. The Y-axis of the *Leg SCS* runs from the AnJC to KJC. The X-axis is normal to the plane containing the KJC, the AnJC and FH. The Z-axis is the cross product of the X and Y axes.

Foot: The origin is FoJC. The X-axis of the *Foot SCS* runs from the CAL to the midpoint between MH1 and MH5. The Y-axis is normal to the plane containing the CAL, MH1 and MH5 pointing cranially. The Z-axis is the cross product of the X and Y axes.

Definition of the eleven joints and their degrees of freedom

From these SCS, the rotations sequences proposed by the ISB (Wu et al. 2002; Wu et al. 2005) were used to describe kinematics during the pushing block phase of eleven joints. These joints are: the thoracic, movement of the thorax versus abdomen (1 degree of freedom, flexion/extension), the rear and front shoulder, movement of the arm versus the thorax (3 degrees of freedom), elbow, movement of the forearm versus the arm (3 degrees of freedom), hip, movement of the thigh versus the pelvis (3 degrees of freedom), knee, movement of the leg versus the thigh (3 degrees of freedom) and ankle, movement of the foot versus the leg (3 degrees of freedom).

Appendix C

Example of calculation of the maximal kinetic energy (KE_{max}) of two limbs

The figure 9 of the present appendix illustrates, in the case of the thigh and leg, why the sum between each maximal KE (for the thigh and the leg) can not be equal to maximal KE of these both segments. Indeed, each peak is not reached at the same time during the movement.

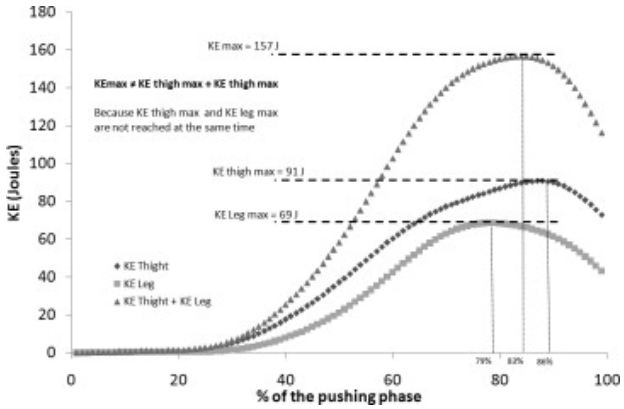

Fig 9